Investigation of *MAT_58 for Modeling Braided Composites

Brina J. Blinzler
University of Akron, Akron Ohio

Robert K. Goldberg
NASA Glenn Research Center, Cleveland Ohio

Wieslaw K. Binienda
University of Akron, Akron Ohio

Abstract

*An in-depth analysis is needed to simulate the impact behavior of triaxially braided composite materials. Before an impact simulation can be generated, all material input parameters must be found. The objective of this work is to use static tests conducted on axial and transverse coupons to determine these input parameters. In particular, analysis methods that capture the architecturally dependent damage observed in these tests in a computationally efficient manner are required. A macromechanical shell element based model for braided composites has been developed, in which the braid architecture is approximated as a series of four parallel laminated composites with varying fiber orientations. The composite damage model *MAT_58, available within LS-DYNA®, is used in this investigation. Careful investigation of the model's global response, and local stress and strain distribution within each element of the composite unit cell are examined parametrically using various input strength parameters. From these studies, relatively small changes in the input parameters have been found to have a significant effect on the overall response, sometimes in non-intuitive ways. Thru this investigation the predictive capability of the developed braid model will be improved and a greater understanding of the functionality of the MAT_58 material model will be obtained.*

Introduction

Textile polymer matrix composite materials are being investigated for use in aerospace applications as a replacement for metals or traditional laminated composites. The goal for this effort is to develop a method to capture the unique failure mechanisms in laminated textile composites. The primary focus for this effort is triaxially braided composites. One application for this type of material is as a jet engine fan blade containment system. In order to create an optimum engine case design, the failure, damage, and deformation needs to be simulated with the use of commercial explicit finite element codes. A design tool was required to capture the structural effect of the braid and damage along fiber bundles while modeling the entire engine case. To balance these needs, a macro scale finite element simulation was developed using the advanced continuum damage mechanics material model *Mat_58 (*Mat_Laminated_ Composite_Fabric) to account for unique structural effects [Ref. 1]. For these aerospace applications the model needed to accurately simulate the textile composite under both static loading and impact situations. This effort looked at a triaxially braided composite with a [0°/+60°/-60°] layup. Taking efficiency into account, the material was modeled as a membrane and the structure was made up of traditional four noded shell elements. The unique way the fiber architecture was incorporated into the shell elements will be discussed later. There has been a significant amount of research conducted in textile composite modeling and analysis. In most of the previous research homogenized material properties were used. For example Tanov

and Tabiei used a representative volume cell approach which assigned homogenized material properties to the model elements [Ref. 2]. These types of approaches do not directly account for the textile architecture in the finite element model and work well for small yarn sizes but lack the ability to capture damage in a composite with larger yarn sizes. It has been noted in experimental impact testing, failure in some textile composites propagates in the fiber directions [Ref. 3]. In order to simulate this unique failure propagation, the textile architecture should be directly simulated in the finite element model. This paper will discuss a method developed to capture this unique textile failure.

Background

Matzenmiller developed a constitutive model for anisotropic damage of fibrous composite materials with non-ductile matrices [Ref. 4]. The method used continuum damage mechanics theory in the material axis system to approximate damage initiation and ultimate material failure. Each lamina was assumed to be a unidirectional composite and any non linearity was assumed to be due to damage mechanisms. The development of damage was completely dependent on the stress and strain states of the individual unidirectional lamina. Matzenmiller then used the Hashin failure criteria which determined a failure envelope based on the five strength properties of the unidirectional lamina: longitudinal tension, longitudinal compression, transverse tension, transverse compression, and shear strengths [Ref. 5]. The equations used in *MAT_58 reflect the Matzenmiller method and assumptions [Ref. 1].

Material	**T700 – PR520**	**T700 - 3502**
Material Parameter Name (LS-DYNA® name)	*Value (unit)*	*Value (unit)*
Axial Modulus (EA)	51.37 (GPa)	51.37 (GPa)
Transverse Modulus (EB)	25.03 (GPa)	25.03 (GPa)
In Plane Shear Modulus (GAB)	18.96 (GPa)	18.96 (GPa)
In Plane Poisson Ratio (PRBA)	0.071	0.071
Axial Tensile Failure Strain (E11T)	0.0216	0.0151
Axial Compressive Failure Strain (E11C)	0.018	0.01
Transverse Tensile Failure Strain (E22T)	0.0168	0.01
Transverse Compressive Failure Strain (E22C)	0.011	0.068
In Plane Shear Failure Strain (GMS)	0.024	0.02
Axial Tensile Stress at Failure (XT)	1044.59 (MPa)	607.45 (MPa)
Axial Compressive Stress at Failure(XC)	377.09 (MPa)	363.37 (MPa)
Transverse Tensile Stress at Failure (YT)	361.99 (MPa)	68.95 (MPa)
Transverse Compressive Stress at Failure (YC)	344.75 (MPa)	243.39 (MPa)
In Plane Shear Stress at Failure (SC)	307.31 (MPa)	224.09 (MPa)
Stress Limiting Parameter for Axial Tension (SLIMT1)	0	0
Stress Limiting Parameter for Transverse Tension (SLIMT2)	1	1
Stress Limiting Parameter for Axial Compression (SLIMC1)	0	0
Stress Limiting Parameter for Transverse Compression (SLIMC2)	0	0
Stress Limiting Parameter for Shear (SLIMS)	0	0

Table 1: Input Parameters

The inputs for the material model are listed in Table 1. The material inputs required by this model are unidirectional strength and stiffness properties. There are five exceptions. The SLIM inputs are not related to mechanical properties. The SLIM inputs are known as stress limiting factors. These stress limiting factors define the amount of additional stress an integration layer can take after the ultimate strength has been reached. A SLIM of one would allow no further stress in the defined direction after reaching ultimate strength and cause the material to act like a perfectly plastic material. SLIM values less than one simulate the material carrying a percentage of stress after hitting ultimate strength. In the model used in this paper a SLIMT2 of one is used. This effectively simulates a perfectly plastic situation when a fiber bundle in the composite reaches ultimate tensile strength in the transverse direction.

Approach

Previous research on this topic was conducted by Cheng and Littell [Ref. 6, 7]. Their analytical model discretized the braided composite into a series of parallel shell elements. Each element in this series was modeled as a laminated composite. This allowed for architecturally dependent damage to be modeled while maintaining a large unit cell for efficiency. This model was based on the identification of the repeating unit cell within the triaxial braid architecture seen in Figure 1 (a). The unit cell was further divided into four subcells: A, B, C, and D noted in Figure 1 (b). These four elements were the building blocks of the model and were repeated in both in-plane directions until the desired size was created. The subcells divided the braid architecture into four areas that individually were approximated as uniaxial laminated composites. This can be seen in Figure 1 (c). The braided composite is composed of six layers which can be seen in Figure 2. In this figure the subcell shifting through the thickness of the unit cell was done to account for the nesting effect noted in experimental samples [Ref. 3].

The braid architecture was incorporated in this model by using equivalent unidirectional composite properties found as a result of laboratory experiments. The unidirectional lamina properties are not known for a braided composite and cannot be directly measured. The equivalent unidirectional properties seen in Table 1 were back calculated from the experimental results using micromechanics equations and classical lamination theory. Further explanation of the equivalent unidirectional properties formulation can be found in Ref. 5. There are several advantages for this analytical model. One advantage is that the constitutive model being used is a continuum damage mechanics model. This quality is important for impact analysis. Another advantage is that the experimental data required for the model comes only from the triaxially braided composite samples; no additional inputs are required. In addition, the model is computationally efficient, and it can be used to model large components.

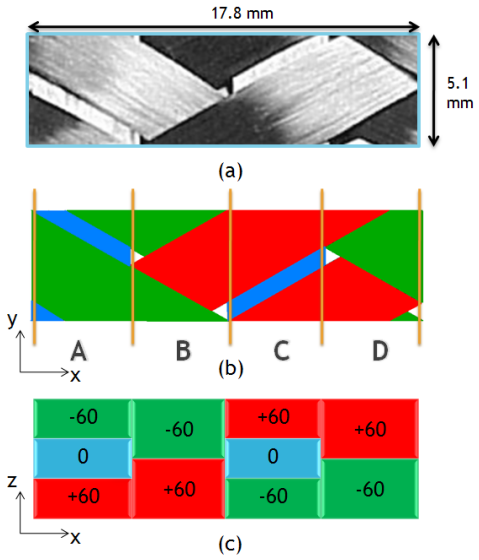

Fig. 1: Identification of the unitcell a)specimen photograph, b)four shell elements (A,B,C,D), c)through thickness integration

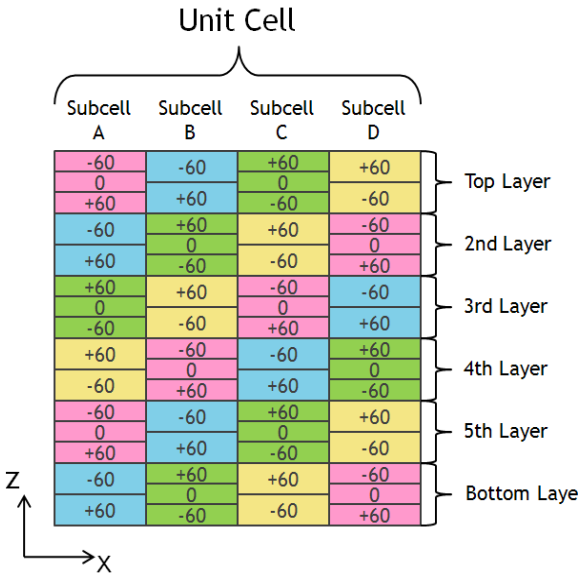

Fig. 2: Through thickness view of shell layers element braided composite unit cell

The shell element formulation allows each integration layer to have a weight factor and thickness. The braided material consists of [0°/+60°/-60°] degree fibers. The zero degree fiber bundles are referred to as axial fiber bundles and the plus and minus sixty degree fiber bundles are referred to as bias fiber bundles. In this case all layers were assigned the same thickness but the zero degree fibers were assigned twice the weight factor of the bias fibers because the zero degree fiber bundles contain two times the amount of carbon fibers as the bias bundles. After analyzing the effects of these inputs, it was determined that changing the thickness of the layer is negligible for this case. The weight factor of the layer contributes only slightly more than the thickness.

Static simulations were conducted to accurately characterize the material and structure. The axial tension and transverse tension simulations seen in Figure 3 were developed to mimic experimental coupon tests. For these static simulations, the nodes at the very top were fixed. This is noted with black crosses in the figure. Displacement in the static simulations was applied to the nodes at the bottom in the negative Y direction while motion for these nodes was constrained in X and Z. The colorful arrows in Figure 3 are showing the amount of displacement near the beginning of the simulation. The stress-strain curves for these simulations were defined by averaging the elemental stresses and strains for the bottom six rows of elements in each model. This is similar to the previous methods used to create stress-strain curves.

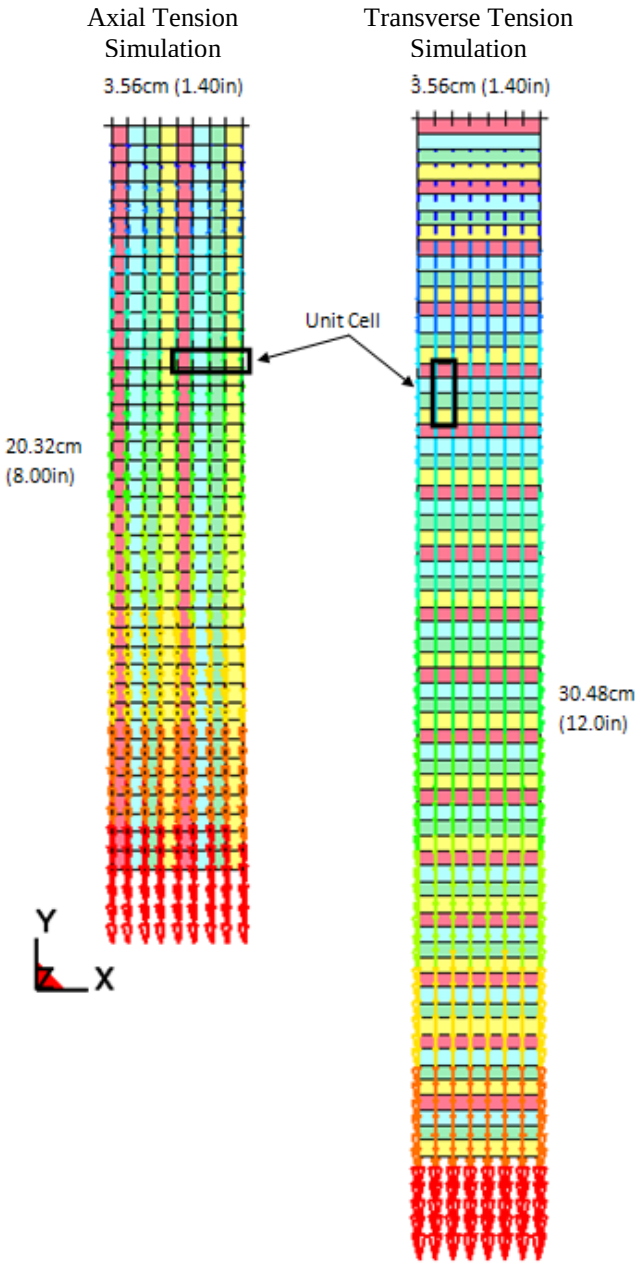

Fig. 3: Simulation Schematics

Parametric studies were conducted to aid in modifying previous assumptions and developing a method of modeling based on experimental data that will capture the differences seen in two triaxially braided composites tested. The two composites that were studied were T700/PR520 and T700/3502, whereT700 refers to Toray's TORAYCA T700s carbon fiber, PR520 refers to Cytec's CYCOM PR 520 resin, and 3502 refers to Hexcel's 3502 resin. The interesting thing was that for T700/PR520 while elastic stiffness properties were the same the nominal strains were different. In order to completely understand the model and to accurately predict failure damage patterns and velocity a complete understanding of how the material inputs affect the simulation results had to be achieved.

In order to examine how each of the strength properties (XT, E11T, XC, E11C, YT, E22T, YC, E22C, SC, and GMS from Table 1) affected the failure of the braid model, a full diagnostic was conducted. Axial and transverse tension simulations from Figure 3 were used in this parametric study. The five strengths mentioned above were varied along with their corresponding failure strains. For example, when shear strength was increased 25 percent, shear failure strain was also increased 25 percent to keep the elastic modulus constant. Both the original six layer and a new single layer model were examined with strength values varied up and down at increments of 25 percent. The strengths and failure strains were increased 25 and 50 percent, and decreased 25 and 50 percent for each variation. From this diagnostic, the primary and limiting parameters were identified. The parametric study was first conducted for the baseline simulation, which was the full six layer nested model. A single layer simulation (Figure 4) was developed to help verify the results and compare with the experimental single layer test. Following this, a parametric study was conducted with both the single layer model and a six layer non-nested model (Figure 5). The six layer non-nested model was used to verify the single layer results and compare with the previous study.

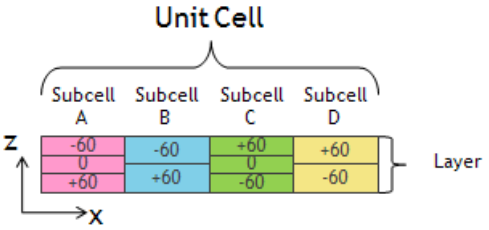

Fig. 4: Single Layer Through Thickness

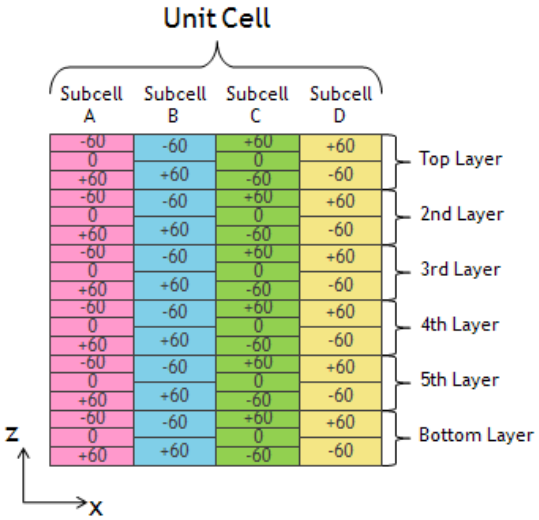

Fig. 5: Six Layer Non-nested Through Thickness

Results

In order to capture the unique failure mechanisms of the triaxially braided composites some of the model assumptions may need to be modified. The model sensitivity must be fully understood to scientifically modify these assumptions. A parametric study was conducted to describe the model sensitivity in detail. There were four sets of simulations run during the course of the parametric study: the baseline parametric study, the single layer verses baseline comparison, the single layer parametric study, and the non-nested comparison. The baseline parametric study was conducted first. Below are the stress-strain graphs which show the effects of the changes to the input parameters in the baseline model. During each of these studies, primary failure drivers were identified for the different inputs for the composite materials. The primary failure driver for these studies was defined as the uniaxial input strength which created the largest change in global output strength and stiffness. Uniaxial shear strength was identified as the primary driver for both axial tension specimen failure and transverse tension specimen failure for the T700/PR520 composite simulation (Figures 7 and 8).

Test data noted in Figures 7-18 is from experimental composite coupon tests [Ref. 3]. The accuracy of the test data for the transverse tension tests for both composites is in question. It has been proposed that there is a significant amount of artificial nonlinearity resulting from ungripped bias fibers [Ref. 3]. Because these composites are quasi-isotropic the experimental transverse tension strength and stiffness should be similar to the strength and stiffness of the axial tension test.

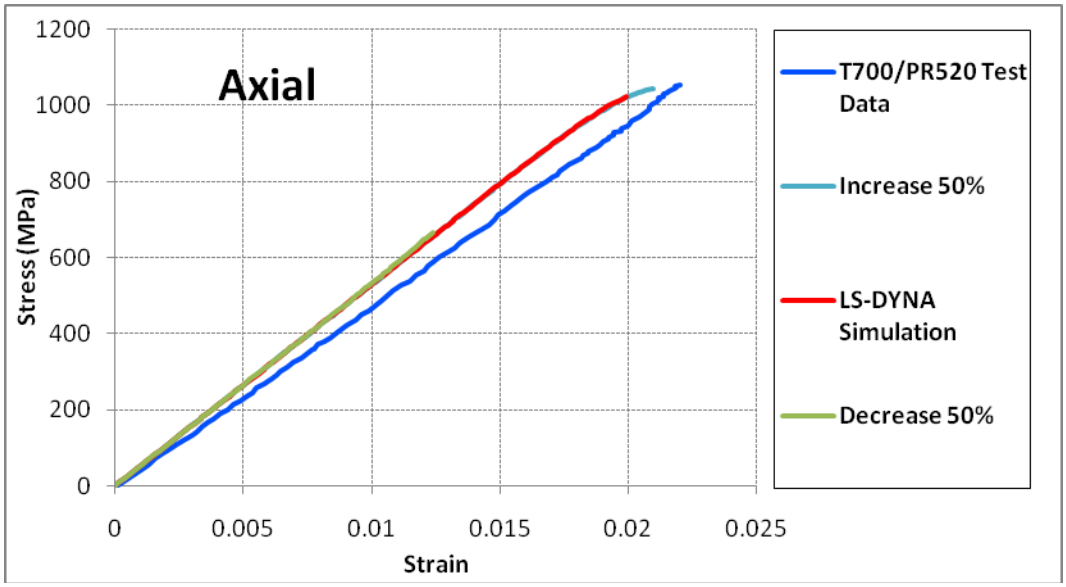

Fig. 7: Baseline Parametric Study T700/PR520 with Shear Strengths Varied for the Axial Tension Simulation

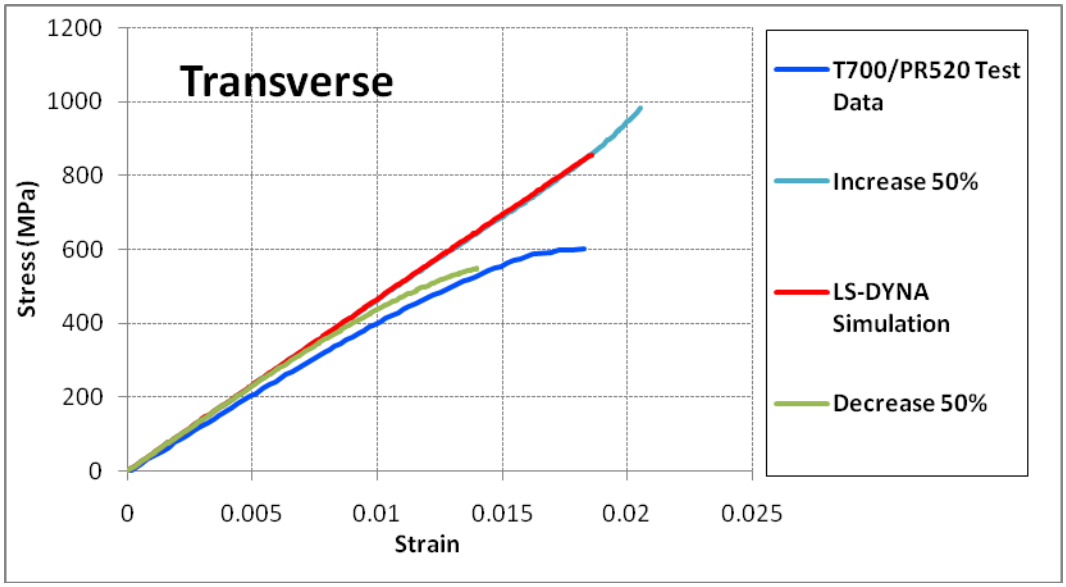

Fig. 8: Baseline Parametric Study T700/PR520 with Shear Strengths Varied for the Transverse Tension Simulation

Uniaxial longitudinal tension strength was identified as the primary failure driver for the axial tension specimen failure for the T700/3502 composite simulation (Fig. 9). Uniaxial shear strength was identified as the primary driver for transverse tension specimen failure for the

T700/3502 composite simulation (Fig. 10). This was different from the T700/PR520 composite and was due to the difference in the ratio of longitudinal strength to other strengths.

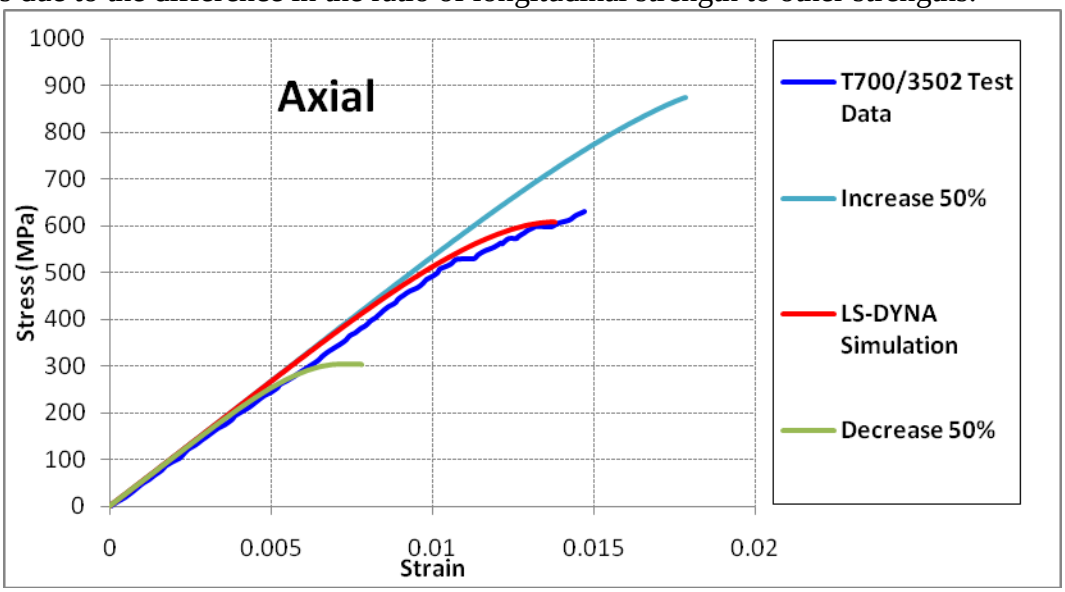

Fig. 9: Baseline Parametric Study T700/3502 with Longitudinal Strengths Varied for the Axial Tension Simulation

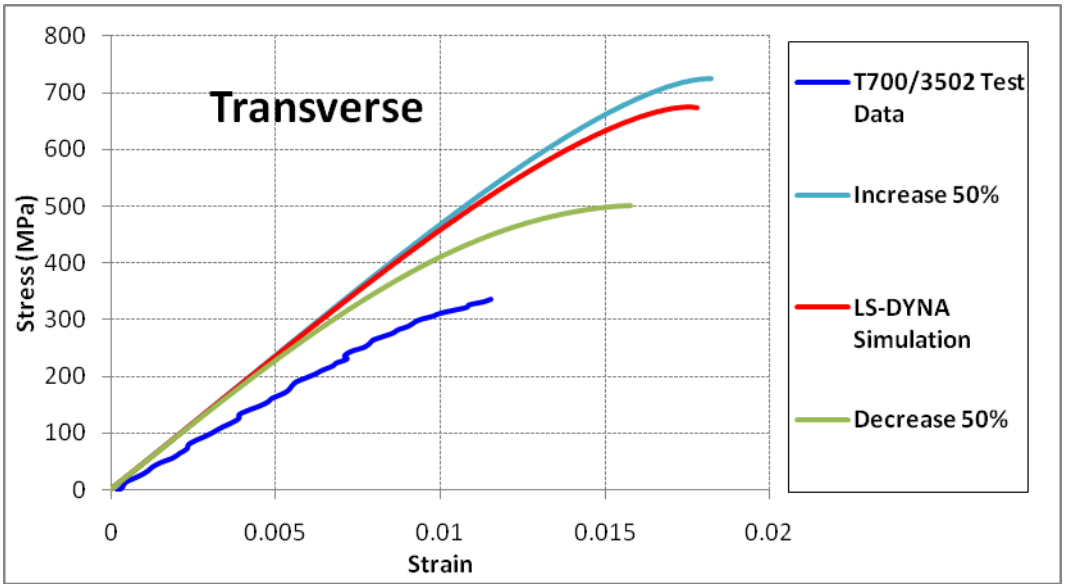

Fig. 10: Baseline Parametric Study T700/3502 with Shear Strengths Varied for the Transverse Tension Simulation

After the baseline parametric study was completed the single layer verses baseline comparison was conducted. This was originally done to validate the baseline parametric study, but ended up prompting further research when the results were seen to differ greatly. Overall the single layer axial tension simulation of T700/PR520 was less stiff and weaker than the six layer simulation (Figure11). Subcells A and C followed the six layer curves and subcells B and D were significantly weaker. The resulting unit cell average had a much lower stiffness and strength than the six ply simulations. The single layer transverse tension simulation of T700/ PR520 (Figure 12) was also less stiff than the six layer simulation. The curve of subcells A and

C were closer to the stiffness of the six layer simulation than the average and the curve of subcells B and D were far weaker. These differences in the single layer simulations were attributed to the behavior of the zero degree fibers. Because of the nested nature of the six layer model, all subcells contained the same amount of zero degree fibers. However, in the single layer simulations this was not the case. Subcells B and D contained no zero degree fibers in the single layer simulations. Due to the lack of strength from zero degree fiber layers, the single layer axial tension simulation had a decreased stiffness and strength and the single layer transverse tension simulation had a decreased strength.

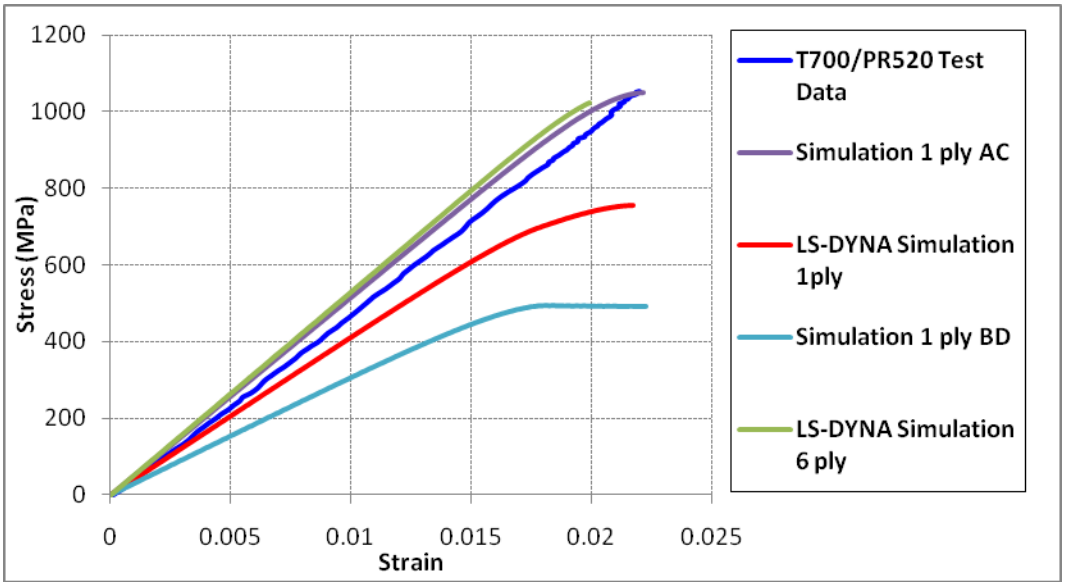

Fig. 11: Single Layer Comparison T700/PR520 for the Axial Tension Simulation

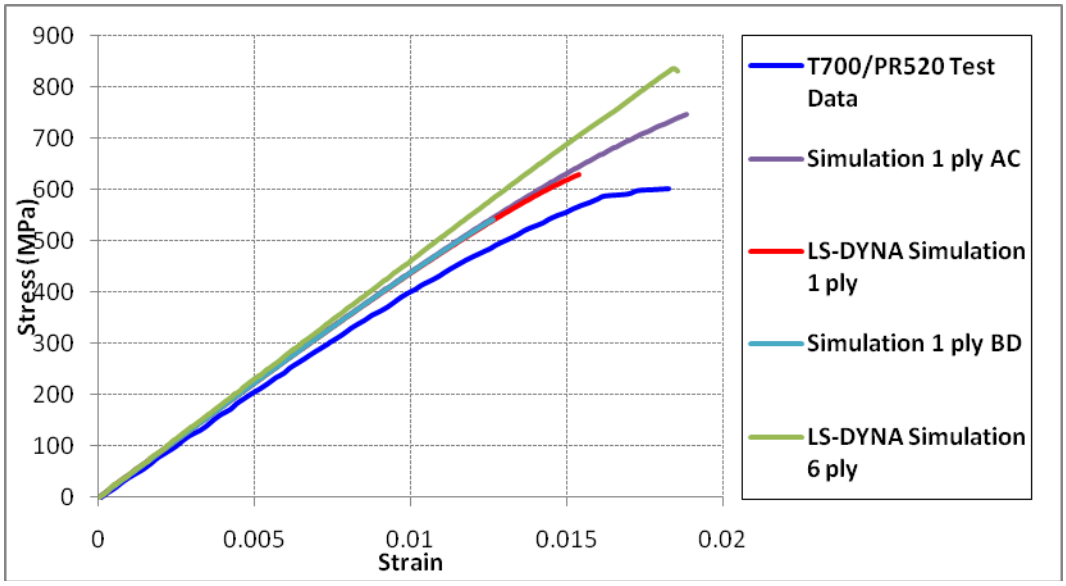

Fig. 12: Single Layer Comparison T700/PR520 for the Transverse Tension Simulation

The single layer axial tension simulation of T700/3502 (Figure 13) was also less stiff than the baseline simulation. Again, the curve for subcells A and C was in line with the six layer simulation but the curve for subcells B and D was much less stiff. The single layer transverse tension simulations of T700/3502 (Figure 14) had the same stiffness but were weaker than the six layer simulations.

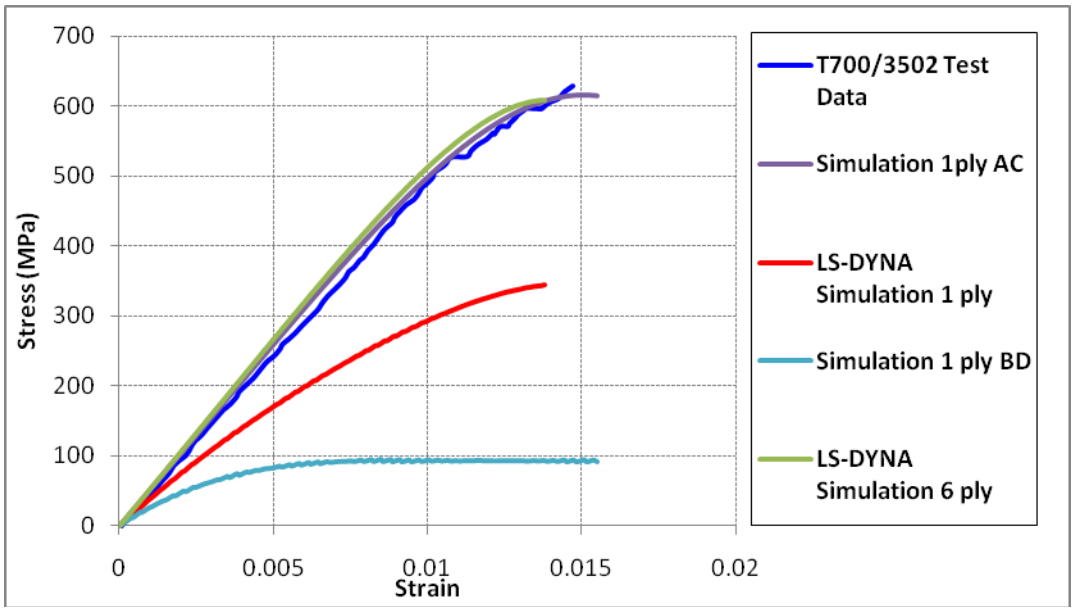

Fig. 13: Single Layer Comparison T700/3502 for the Axial Tension Simulation

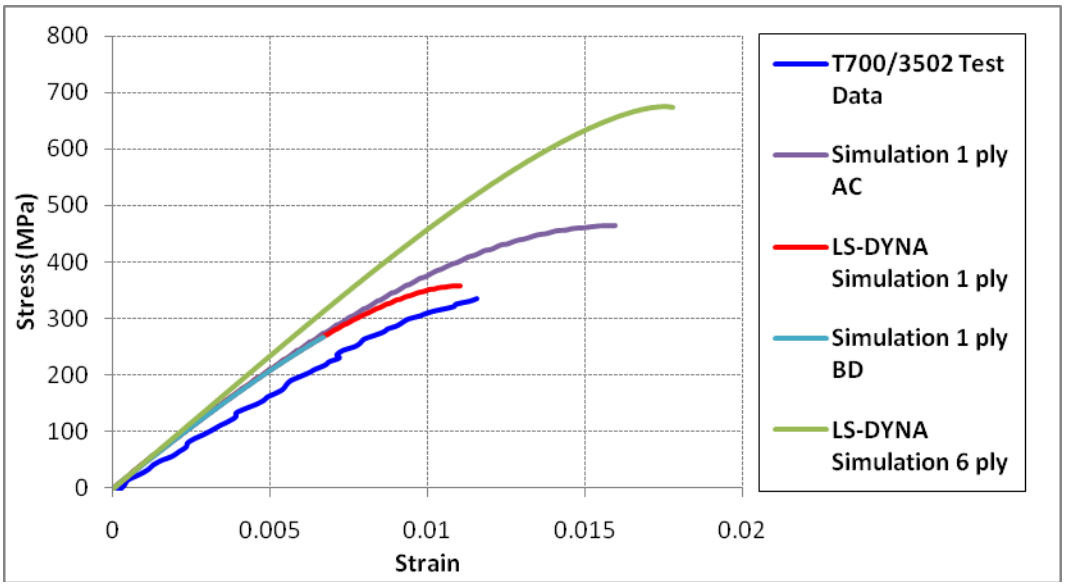

Fig. 14: Single Layer Comparison T700/3502 for the Transverse Tension

After the differences were noted in the single layer comparison, a single layer parametric study was conducted to characterize the effects of changing the strengths on subcells with and without zero degree fiber layers. In the single layer parametric study the T700/PR520 composite was analyzed first. For this analysis, the uniaxial longitudinal tension strength and failure strain were varied first. When the uniaxial longitudinal tension strength and failure strain (XT & E11T) were varied, the axial tension simulation was affected significantly while the transverse tension simulation was not. During the axial tension simulation, when the uniaxial longitudinal

tension strength and failure strain were increased, the global strength increased and the global strength decreased when they were decreased. However, during the transverse tension simulation, there was no significant change. There was only a small decrease in the global strength when the uniaxial longitudinal strength and failure strain were decreased by 50 percent. Next, the uniaxial transverse tension strength and failure strain were varied. When the uniaxial transverse tension strength and failure strain (YT & E22T) were varied, both the axial tension and the transverse tension simulations were affected. During the axial tension simulation, the curve followed a similar path to the baseline, but as the uniaxial transverse tension strength and failure strain decreased the global strength decreased and the stress at which the transition to nonlinearity occurs also decreased. During the transverse tension simulation, when the uniaxial transverse tension strength and failure strain increased the global strength and stiffness of the curve increased and when the uniaxial strength and failure strain decreased the global strength and stiffness decreased. Finally, the uniaxial shear strength and failure strain were varied. When the uniaxial shear strength and failure strain (SC & GMS) were decreased both the axial tension and transverse tension simulations were significantly affected. There was less change when the uniaxial shear strength and failure strain were increased. During the axial tension simulation, when the uniaxial shear strength and failure strain were decreased the global strength decreased and when the uniaxial strength and failure strain were increased the global strength increased. During the transverse tension simulation, when the uniaxial shear strength and failure strain decreased the global strength and stiffness decreased and when the uniaxial strength and failure strain increased the global strength and stiffness increased.

The T700/3502 composite was analyzed second. For this analysis, the uniaxial longitudinal tension strength and failure strain were varied first. When the uniaxial longitudinal tension strength and failure strain (XT & E11T) were increased and decreased, both the axial tension and transverse tension simulations were affected. There was some change when the uniaxial longitudinal tension strength and failure strain were increased. During both simulations when the uniaxial strength and failure strain decreased, the global strength decreased significantly. Next, the uniaxial transverse tension strength and failure strain were varied. When the uniaxial transverse tension strength and failure strain (YT & E22T) were varied, both axial and transverse tension simulations were affected. During the axial tension simulation when the uniaxial transverse tension strength and failure strain increased, global stiffness increased, and when the uniaxial strength and failure strain decreased the global stiffness decreased. During the transverse tension simulation when the uniaxial transverse tension strength and failure strain increased, global strength and stiffness increased, and when the uniaxial strength and failure strain decreased the global strength and stiffness decreased. Finally, the uniaxial shear strength and failure strain were varied. When the uniaxial shear strength and failure strain (SC & GMS) were varied, both axial and transverse tension simulations were affected. During the axial tension simulation, when the uniaxial shear strength and failure strain increased the global strength increased and when the uniaxial strength and failure strain decreased the global strength decreased. During the transverse tension simulation, when the uniaxial shear strength and failure strain increased the global strength and stiffness increased significantly and when the uniaxial strength and failure strain decreased the global strength and stiffness decreased significantly. Comparing all these variations, primary failure drivers were found for the transverse tension and axial tension tests for both composites.

From the single layer parametric study, primary failure drivers were identified. The stress-strain graphs displaying these primary failure drivers are seen in Figures 15-18. Uniaxial shear

strength was identified as the primary driver for both axial tension specimen failure and transverse tension specimen failure for the T700/PR520 composite (Figures 15 and 16). These results were similar to those noted in the parametric study involving the six ply laminate.

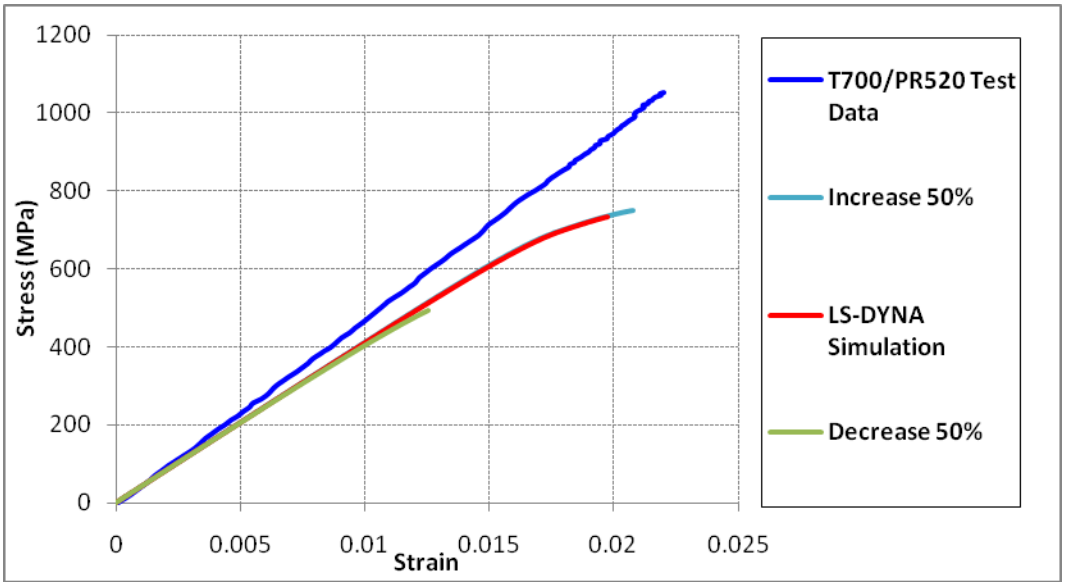

Fig. 15: Single Layer Parametric Study T700/PR520 with Shear Strengths Varied for the Axial Tension Simulation

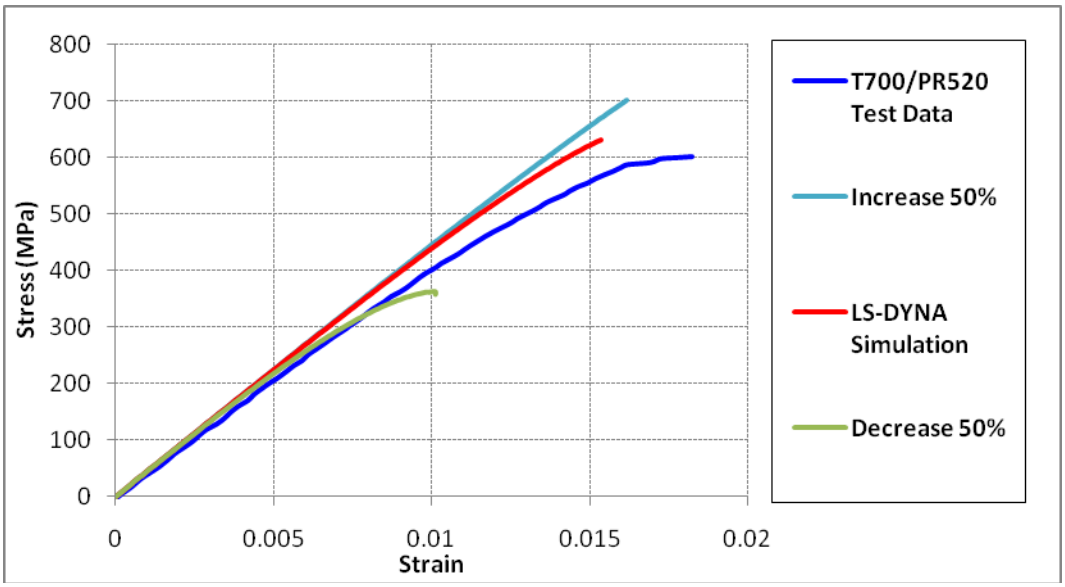

Fig. 16: Single Layer Parametric Study T700/PR520 with Shear Strengths Varied for the Transverse Tension Simulation

The uniaxial longitudinal strength was identified as the primary failure driver for the axial tension specimen failure for the T700/3502 composite simulation (Figure 17). The uniaxial shear strength was identified as the primary driver for transverse tension specimen failure for this composite (Figure 18). These results are also similar to those noted in the parametric study involving the six ply laminate.

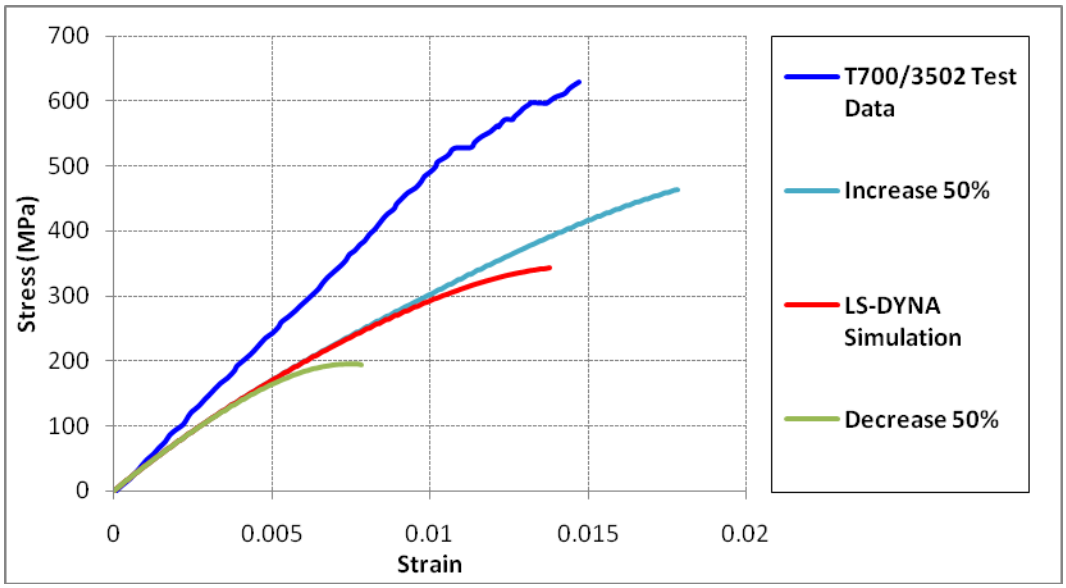

Fig. 17: Single Layer Parametric Study T700/3502 with Longitudinal Strengths Varied for the Axial Tension Simulation

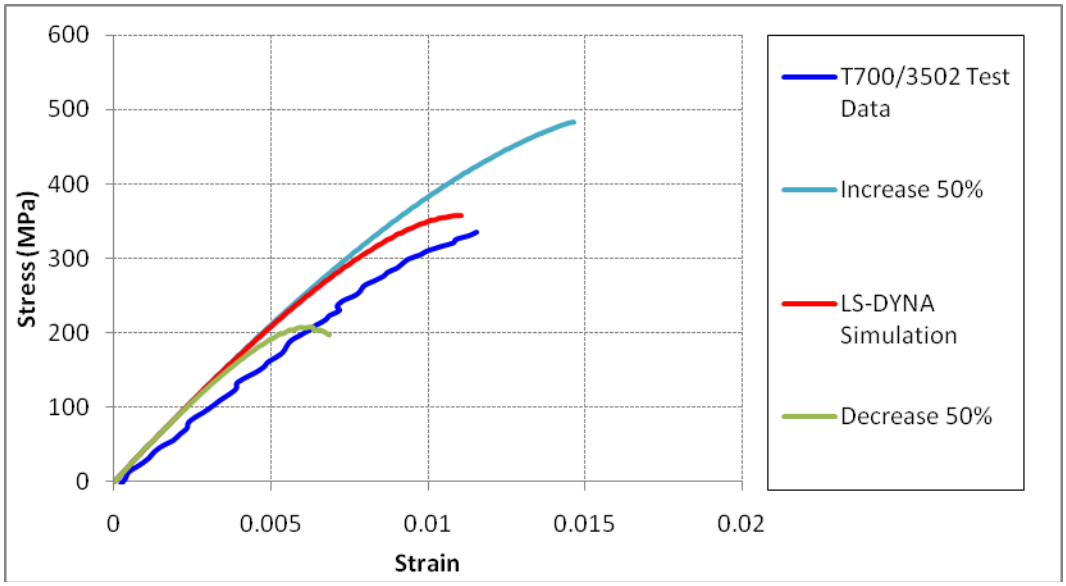

Fig. 18: Single Layer Parametric Study T700/3502 with Shear Strengths Varied for the Transverse Tension Simulation

After the single layer parametric study, six layer non-nested simulations were run to validate the data from the single layer study. The six layer non-nested model behaved very similar to the single layer model. For all four of the T700/PR520 and T700/3502 composite simulations the stress strain curves were nearly identical for the six layer non-nested and the single layer models. In order to identify why the different materials had different simulation responses and different input sensitivity, a number of strength ratios were calculated. In situ uniaxial strengths were compared in the form of tables of ratios (Tables 2 and 3). This showed that the in situ shear and transverse strengths of the T700/PR520 composite were similar while the axial strength was much larger (Table 2). This meant that the specimens could be near failure in either the shear or transverse directions and small changes in uniaxial strength could easily tip the scales. This also

helped explain why shear strength and stiffness plays such a significant role in failure in both the axial and transverse tension simulations for the T700/PR520 composite material. This was not the case for the T700/3502 composite. The transverse strength is much lower and the shear strength is much higher in comparison. The uniaxial strengths for the two different composites were also compared by ratios (Table 3). This comparison makes clear the large relative difference in the uniaxial transverse tensile strengths and the small relative difference in the uniaxial shear strengths. This relative difference is important because uniaxial shear strength appears to play a large role in the failure of both composites.

	T700/PR520	T700/3502
ratio (YT/XT)	0.35	0.11
ratio (SC/XT)	0.29	0.37
ratio (SC/YT)	0.85	3.25

Table 2: Composite Strength Ratios

ratio(XT) T700-3520/T700-PR520	0.58
ratio (YT) T700-3520/T700-PR520	0.19
ratio (SC) T700-3520/T700-PR520	0.73

Table 3: Composite Strength Ratios

Conclusion

During this effort to capture the unique failure mechanisms of laminated textile composites, several steps were taken to ensure that the simulation output is a direct result of scientifically implementing experimental data. Through this effort a deeper understanding of the sensitivity of the macromechanical model has been obtained. The parametric studies and layer level integration point analysis are crucial in the definition of a quasi-empirical formula to capture material failure. This empirical formula's more accurate input parameters are being developed exclusively from experimental data. The formula is being implemented in a program that requires experimental data for input, and outputs a set of *Mat_58 material cards. These material cards can then be used in an LS-DYNA® analysis. Through this effort the predictive capability of the developed braid model is being improved. This method will create a more accurate and easy to use modeling tool for textile composite materials.

References

1. Hallquist, J.O. et al, "LS-DYNA® Keyword User's Manual", Livermore Software Technology Corporation, Livermore, CA, May 2007.
2. Tanov, R., Tabiei, A. "Computationally Efficient Micromechanical models for Woven Fabric Composite Elastic Moduli". J. Appl. Mech. 68. 2001.
3. Roberts, G. et al. "Impact Testing and Analysis of Composites for Aircraft Engine Fan Cases". NASA TM 211493. 2002.
4. Matzenmiller, A., Lubliner, J., Taylor, R.L. "A constitutive model for anisotropic damage in fiber-composites", University of California at Berkeley. Berkeley, California. 1994.
5. Hashin, Z., "Failure Criteria for Unidirectional Fiber Composites", J. Appl. Mech. 47, 329. 1980.
6. Cheng, J., "Material Modeling of Strain Rate Dependent Polymer and 2D Triaxially Braided Composites", Ph.D. Dissertation. University of Akron. Akron, Ohio. 2006.
7. Littell, J., "The Experimental and Analytical Characterization of the Micromechanical Response for Triaxial Braided Composite Materials", Ph.D. Dissertation. University of Akron. Akron, Ohio. 2008.